Journal of Information Systems Engineering and Management
2025, 10(37s)
e-ISSN: 2468-4376
https://www.jisem-journal.com/

Research Article

Investigation of Microstructure Evolution in Wire Arc Additive Manufacturing of Steel Followed by Hot Forming

Nabeel Alawi Albahadli [1], Abdul Sameea Jasim Jilabi [2], Hayder Aljuboori [3]
[1]*Faculty of Engineering, University of Kufa -Iraq*
[2,3] *College of Materials Engineering, University of Babylon -Iraq.*
[1] *Corresponding author: nabeel.albahadli@uokufa.edu.iq*
[2] *sameeakilabi@gmail.com*
[3] *mat.hayder.abadhassan@uobabylon.edu.iq*

ARTICLE INFO

Received: 26 Dec 2024

Revised: 14 Feb 2025

Accepted: 22 Feb 2025

ABSTRACT

Metal Inert Gas (MIG)-based weld deposition process, a subset of wire arc additive manufacturing (WAAM), has received significant attention in the field of additive manufacturing (AM). This technique is favored for its ability to efficiently produce complex, dense and fully functional metallic components. Its key benefits include high deposition rates, material and energy efficiency, lower investment costs, and simplified setup requirements, making it an attractive option for metallic AM. This study focuses on exploring the synergistic effects of combining two processing practices: additive manufacturing and hot forming with varying hammer strokes (3HS, 5HS, and 7HS) on steel components. The investigation utilizes the WAAM technique with a MIG setup to create components on a low alloy steel substrate, employing diverse deposition patterns. Experiments were conducted using fully automated MIG welding on a low alloy steel substrate with ER70S-6 copper-coated steel wire. Samples were built using five different deposition patterns: longitudinal, transverse, right network, oblique, and oblique network. To evaluate the samples, various examinations were performed, including optical microscopy and scanning electron microscopy. The results revealed that the samples built with the different deposition patterns showed a diversity of microstructure in different regions along the cross-section of the additives. Microscopy generally showed that the primary constituent of the dominant structure in the additive material was lamellar pearlite with grain boundary ferrite, accompanied by a smaller fraction of ferrite grains. Hot forging led to a notable reduction in the interlamellar spacing within the pearlite colonies, and in both grain boundary ferrite and ferrite grains across the additives.

Keywords: Additive manufacturing (AM), 3D printers' technology, Arc welding, Steel, Hot forging.

1. INTRODUCTION

Wire and Arc Additive Manufacturing (WAAM) is a transformative technology that constructs metal components layer by layer using an electric arc to fuse a continuous wire feed. This method is particularly advantageous for producing complex geometries and customized designs, making it applicable across various industrial sectors. Key aspects of the WAAM process include the optimization of process parameters, the influence of wire types, and the innovative use of variable layer heights [1]. WAAM has a rich history, dating back to the 1920s, as the process of depositing weld metal to fabricate entire components began. According to ASTM F2792-12a, WAAM is classified as a wire-feed AM method that involves DED and utilizes an electric arc heat source along with metal wire as a raw material. The fundamental concept of WAAM is rooted in automatic welding processes. Over the years, WAAM has been referred to by various names such as rapid prototyping (RP), shape melting (SM), shape welding (SW), shape metal deposition (SMD), solid freeform fabrication (SFF), and even 3D welding, showcasing its versatility and broad applications in AM [2]. Based on the nature of the heat source used in WAAM, there are three primary approaches, as outlined in Figure (1) [3].

Journal of Information Systems Engineering and Management
2025, 10(37s)
e-ISSN: 2468-4376
https://www.jisem-journal.com/

Research Article

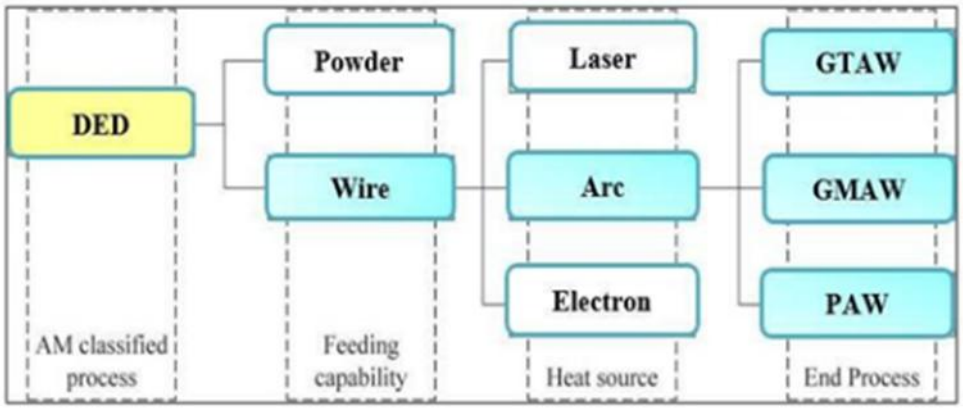

Fig. 1. Typical classification of WAAM [3].

In WAAM, commercially available wires designed for the welding industry are utilized. These wires are typically provided in spooled form and offer a diverse selection of alloys like feedstock materials [4]. Common metals used in WAAM processes, as depicted in Figure (2), include a variety of alloys tailored to meet specific application requirements. These alloys may encompass materials such as stainless steel, aluminum, titanium, nickel-based superalloys, and other specialized alloys suitable for AM through wire arc techniques. The availability of a wide range of feedstock materials in spooled wire form enhances the flexibility and adaptability of WAAM processes, enabling the production of components with varying material properties and characteristics to meet the demands of diverse industrial applications [5]. Gas Metal Arc Welding (GMAW) is a versatile welding process characterized by the continuous feeding of consumable wire electrode and shielding gas through a welding gun. This method, also known as Metal Inert Gas (MIG) or Metal Active Gas (MAG) welding, employs various metal transfer techniques, including globular, short-circuiting, spray, and pulsed spray, each with unique advantages and limitations [6].

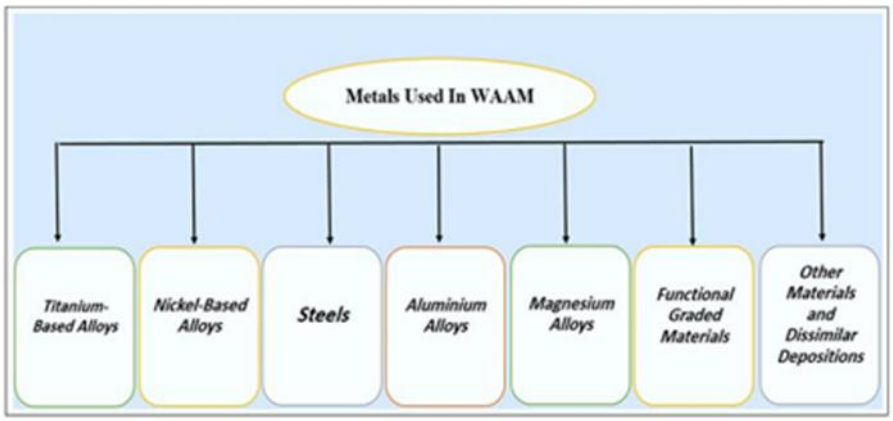

Fig. 2. The metals that are commonly used in WAAM [5].

2. EXPERIMENTAL

Experiments were carried out using an automated MIG welding system shown in Figure (3) to build the samples. Lincoln Electric Power MIG (350MP) machine was utilized as a source of energy. In this work, a CNC (computer numerical control) machine was fabricated to make the welding process fully automated. The experimental procedure started by creating a detailed computer-aided design (CAD) model of the part to be manufactured. Computer-aided manufacturing (CAM) software (3D) was used to generate the corresponding G-code that defines the machining operations.

Journal of Information Systems Engineering and Management
2025, 10(37s)
e-ISSN: 2468-4376
https://www.jisem-journal.com/

Research Article

Fig. 3. An automated MIG welding machine.

Three layers were deposited onto a (12×80×100) mm low alloy steel substrate using Wire Arc Additive Manufacturing (WAAM). The deposition employed 1 mm diameter ER70S-6 filler wire as feedstock and pure CO2 as a shielding gas. The resulting build had dimensions of (9×80×100) mm, as illustrated in Figure 4. The specific WAAM parameters used are detailed in Table 1. Five different deposition patterns are shown schematically in Figure 5. The first pattern was longitudinal, in a direction parallel to the X-axis of the substrate (Figure 4), the second pattern was transverse, in a direction parallel to the Y-axis, and the third pattern was a right network of sequentially longitudinal and transverse lines. The fourth deposition pattern was an oblique at an angle of 45°, while the last pattern was an oblique network at an angle of 45° as well.

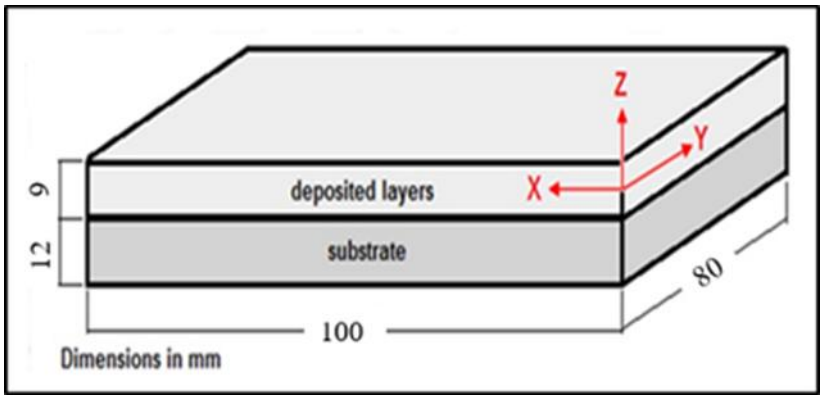

Fig. 4. Deposited layers on the substrate.

Table 1. MIG parameters used with the WAAM process.

Parameters	Value
Welding current	136 A
Welding Voltage	25 V
Wire feeding rate	8 m/min
Travel speed	375 mm/min
Shielding gas	pure CO_2
Gas flow rate	10 l/min
Bead type	Stringy bead
Bead width	9 mm

Journal of Information Systems Engineering and Management
2025, 10(37s)
e-ISSN: 2468-4376
https://www.jisem-journal.com/

Research Article

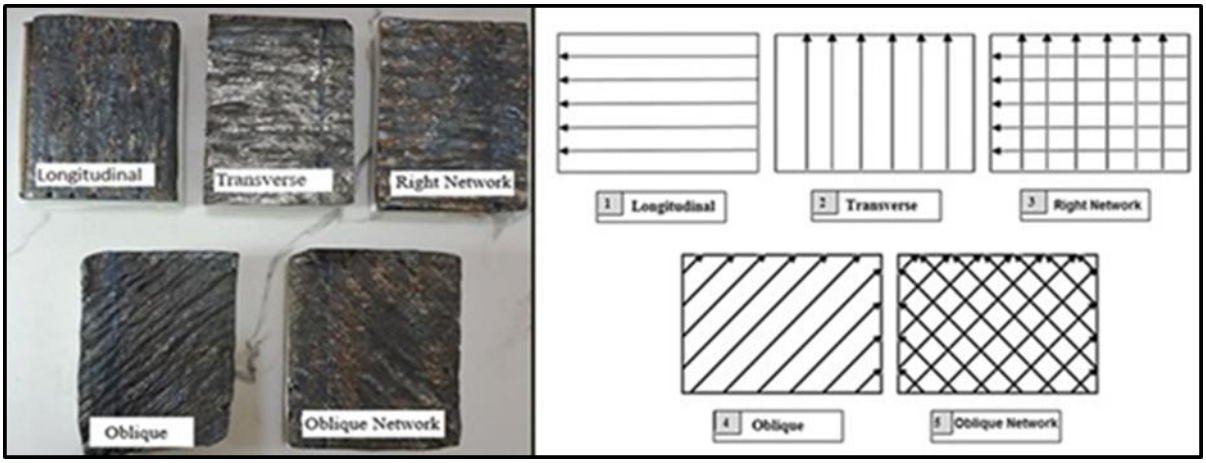

Fig. 5. Deposition patterns of WAAM.

Hot forging was carried out by using the electric forging hammer KALININ (MA-417) with a forging temperature of about 700°C. The forging process was open die schematically shown in Figure 6.

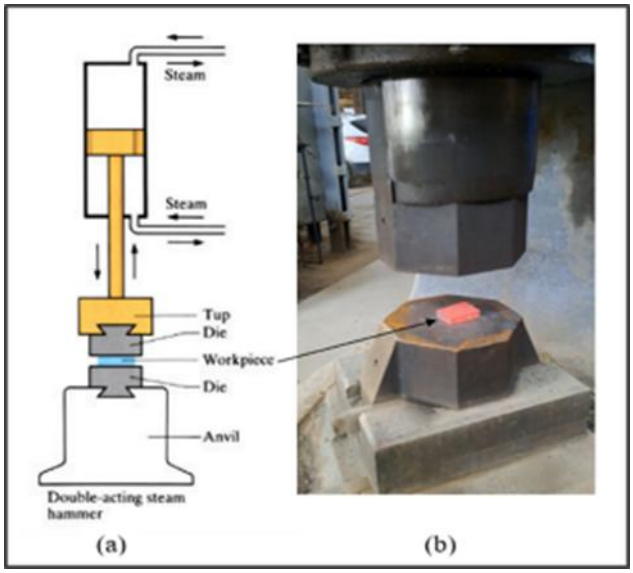

Fig. 6. (a) Schematic representation of open die forging process (b) Open die forging process.

Samples were hot-forged using three different hammer strokes of hot-forging: three, five, and seven hot-forging hammer strokes (HS). The sample was placed in the furnace and heated to the forging temperature, monitoring the temperature with a pyrometer. Once reaching the specified temperature, the sample was carefully transferred from the furnace to the forging hammer. After forging, the sample was allowed to cool gradually in air. All the experimental parameters of the hot forging process of the current study are shown in Table 2.

Table 3. explains the experiments of the current study.

Table 2. Experimental parameters of hot forging.

Parameters	Value
Forging Force	0.750 Ton

Journal of Information Systems Engineering and Management
2025, 10(37s)
e-ISSN: 2468-4376
https://www.jisem-journal.com/

Research Article

Stroke Rate (Frequency)	70 impacts/min
Die Space	800 mm
Stroke Length	600 mm
Die Geometry	Octagonal

Table 3. Experiments of the current study.

Pattern / WAAM		Longitudinal	Transverse	Right Network	Oblique	Oblique Network
		P1	P2	P3	P4	P5
Hot Working	3HS	P136	P236	P336	P436	P536
	5HS	P156	P256	P356	P456	P556
	7HS	P176	P276	P376	P476	P576

3. Characterization And Microscopy

3.1 Optical Microscopic Inspection

Specimens for microstructural analysis were prepared following the standard metallographic techniques, which include the steps outlined below:

1. Cutting: The specimens were cut to an appropriate size to facilitate handling and to detect microstructural variations across different zones.

2. Wet Grinding: The specimen surface was subjected to wet grinding using a rotary disc and emery papers of silicon carbide (SiC) in a sequential order of grades (80 to 1500). After grinding, the specimen was washed with water and dried using hot air.

3. Mechanical Polishing: To remove finer scratches introduced during the grinding process, diamond particle pastes were employed. Polishing was performed sequentially with pastes of 3, 1 and 0.25 µm on specially designed clothes attached to electrically powered rotary discs.

4. Etching: Nital (a mixture of 2% nitric acid and 98% methanol) was used as an etchant to reveal the phases by chemically interacting with different phases at various levels. After etching, the prepared surface was cleaned with alcohol. Finally, an optical microscope was utilized to examine the microstructure and topography of the various regions of both the additive metal and the substrate.

3.2 Scanning Electron Microscopy

SEM images were captured for all prepared specimens to achieve a detailed investigation of microstructures at higher magnifications. The specimens underwent preparation involving suitable paper grinding, polishing and etching with nital solution, following the same procedures used for optical microscopy. Three distinct regions of the additive metal, upper, middle and lower, along with the substrate metal, were analyzed.

4. Results And Discussion

4.1 Microstructure

Journal of Information Systems Engineering and Management
2025, 10(37s)
e-ISSN: 2468-4376
https://www.jisem-journal.com/

Research Article

Microscopic examination along the cross-section of the longitudinally deposited additive material (P1 in Table 3) reveals in Figure 7 a variety of microstructures across various regions (upper, middle and lower regions). The primary constituent of the dominant structure in the additive material is lamellar pearlite with grain boundary ferrite, accompanied by a smaller fraction of ferrite grains. It is clear from Figure 7 that the grain size across the various regions of the three deposited layers was almost similar. However, it is noticed that the ferrite content in microstructure of the lower region was significantly greater than that of the middle and upper regions. This is due to the effect of dilution by the substrate material, which has a higher amount of ferrite content. The dilution effect with the substrate material was evidenced by the study of Al-Roubaiy et al. (2023) [7]. Microscopy across the different regions demonstrates that the filler material used in the AM process encourages the appearance of pearlite despite a low carbon percentage in its chemical composition. This could be attributed to the increased content of alloying elements such as manganese and silicon, leading to an increased fraction of pearlite in the microstructure [8,9]. This is clearly shown in the built-up layer/substrate interface region (Figure 8) which contains more pearlite than the substrate, as a result of dilution. The pearlite colonies in this region appear to have been partially spheroidized as a result of heat required to deposit AM material.

The microstructural analysis conducted through the cross-section of the transversely deposited additive material (P2), depicted in Figure 9, reveals a variety of microstructures in the different regions. Like P1, the microstructure of the additive metal in P2 mainly comprises pearlite colonies with small amounts of grain boundary ferrite, in addition to a smaller fraction of ferrite grains. The structure shape and size in the various regions of this sample, compared to those observed in P1, appeared somewhat coarser. This difference could be attributed to the fact that the increased number of AM runs required to construct layers in the P2 sample (Figure 5) leads to heat accumulation and subsequently lower cooling rates, providing more time for the structure to grow as suggested by Le and Paris (2020) [10].

Microscopic examination of the P3 sample across the various regions reveals in Figure 10 significantly finer microstructures compared to P1 and P2 samples. This could be attributed to the deposition technique employed during AM; this finding aligns with the results reported by Aldalur et al. (2020) [11]. Depositing metal transversely, which requires an increased number of AM runs to be achieved, over the longitudinally deposited metal, enhances heat accumulation, promoting recrystallization. This is consistent with that revealed by Al-Roubaiy et al. (2023) [7]. The transverse deposition leads to increased thermal cycling, allowing partial remelting of the previous longitudinally deposited layers, thus refining the microstructure [12]. The recrystallization process allows the columnar grains to be transformed into fine, equiaxed grains, which benefits the performance of the material [13]. Conversely, while the P3 sample exhibits improved microstructural characteristics, it is essential to take into account that excessive heat accumulation can also lead to undesirable effects, such as some defects like porosity, oxidation and hot cracks if not properly managed. This highlights the delicate balance required in AM processes.

Journal of Information Systems Engineering and Management
2025, 10(37s)
e-ISSN: 2468-4376
https://www.jisem-journal.com/

Research Article

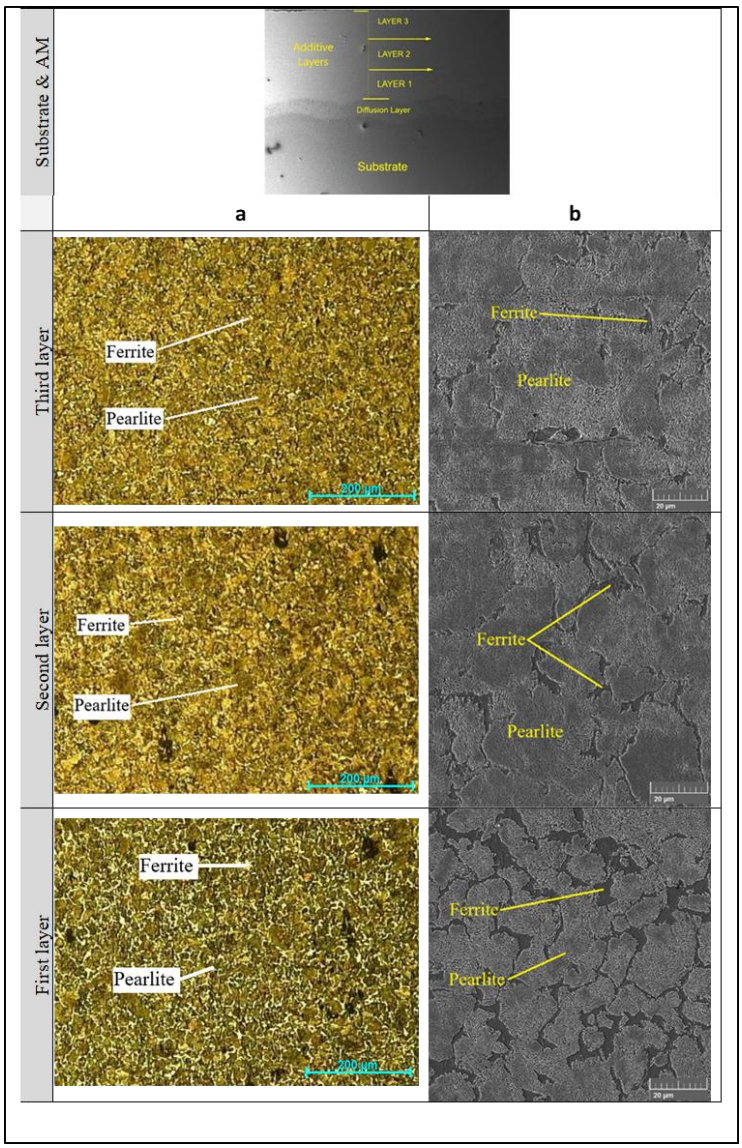

Fig. 7. Micrography of the different regions along the cross-section of the P1 sample using (a): OM and (b): SEM.

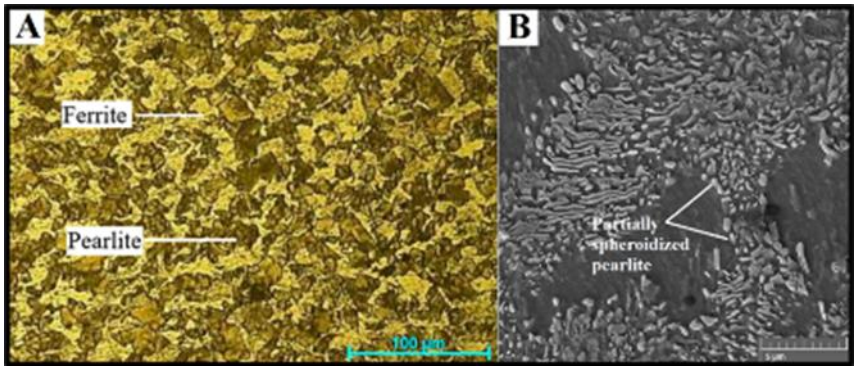

Fig. 8. Microstructure of the built layer/substrate interface region of P1 sample using (A): OM and (B): SEM.

Journal of Information Systems Engineering and Management
2025, 10(37s)
e-ISSN: 2468-4376
https://www.jisem-journal.com/

Research Article

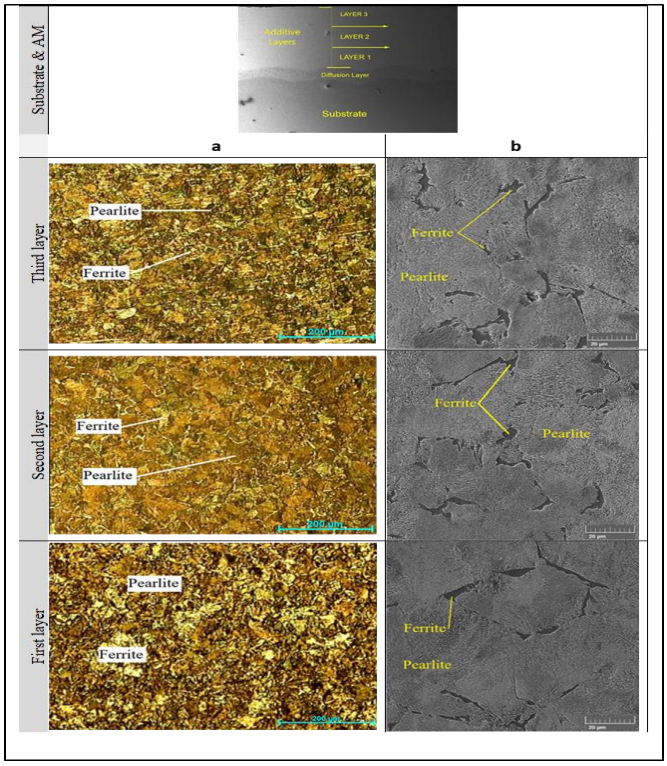

Fig. 9. Micrography of the different regions along the cross-section of the P2 sample using (a): OM and (b): SEM.

The deposition strategy described above, i.e. the repeated heating and cooling cycles of layered deposition in alternating directions, significantly influences the resulting microstructure. This is because each subsequent layer of deposition introduces a thermal cycle that can temper (reheat) and potentially alter the previously deposited layers. With each layer, the material does not have sufficient time to cool down completely before the next layer is deposited. This leads to a gradual increase in temperature in the underlying layers.

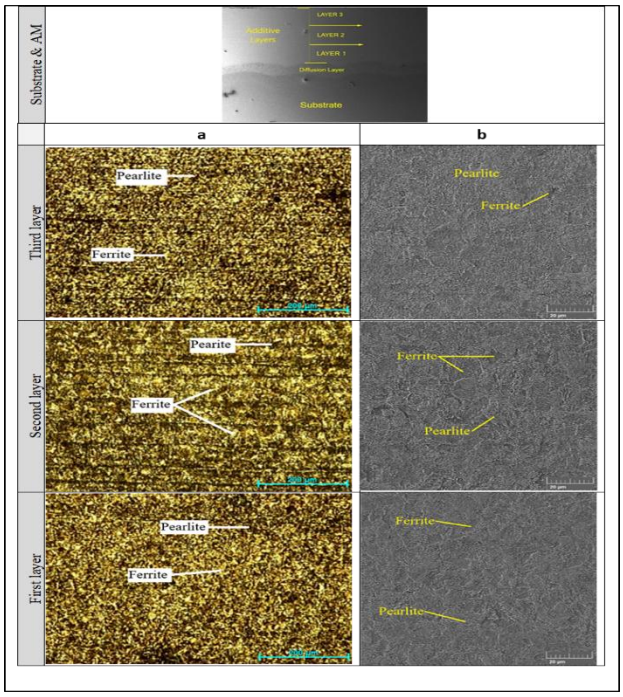

Fig. 10. Micrography of the different regions along the cross-section of the P3 sample using (a): OM and (b): SEM.

Journal of Information Systems Engineering and Management
2025, 10(37s)
e-ISSN: 2468-4376
https://www.jisem-journal.com/

Research Article

Micrography in Figures 11 for the P4 sample reveals that the structure across the different regions was somewhat similar to that of the P1 sample. The primary constituent of the dominant structure along the cross section of the additive material in this sample is also lamellar pearlite with grain boundary ferrite, accompanied by a smaller fraction of ferrite grains.

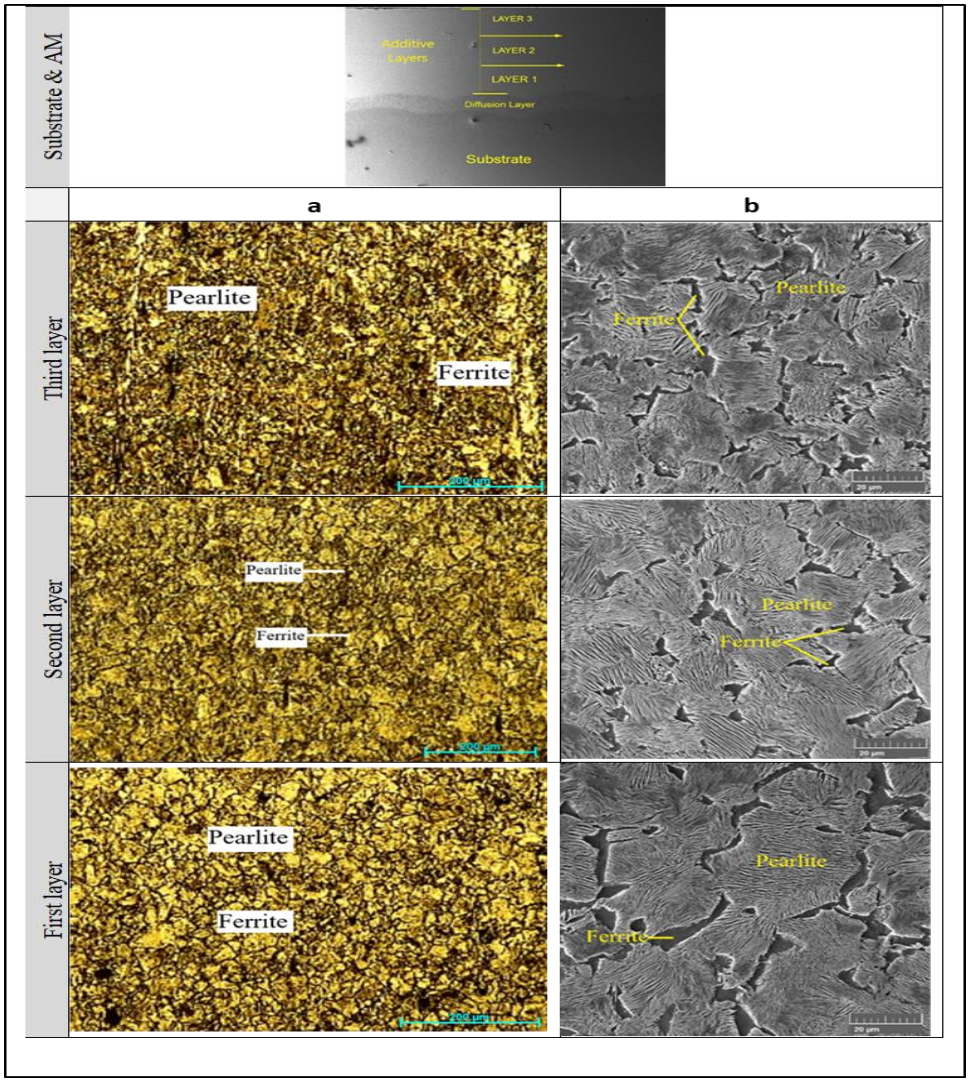

Fig. 11. Micrography of the different regions along the cross-section of the P4 sample using (a): OM and (b): SEM.

The size of the lamellar pearlite colonies across the different regions of this sample is almost similar to that observed in the P1 sample but varies from layer to layer. The lamellar pearlite in microstructure of the additive material of the first layer is noticeably coarser than that of the second layer, which in turn is coarser than that of the third layer. In addition, the pearlite lamellar spacing in this sample is significantly larger than that appeared in pearlite colonies of the previous samples. The variation in size and morphology of the pearlite colonies (and the spacing of the ferrite and cementite lamellae within them) across this additively manufactured sample depends heavily on the cooling rates and recrystallization. In the initial layer, fast cooling by the substrate would indeed result in the formation of coarser pearlite (larger colonies, potentially with wider spacing between the ferrite and cementite lamellae) within larger columnar grains. The subsequent deposited layers provide heat that can cause recrystallization of the columnar grains into equiaxed grains. This heat can also temper the pearlite, potentially coarsening it further.

The preheating effect of the initial layer slows down the cooling rate. This would lead to the formation of finer pearlite (smaller colonies, potentially with narrower lamellae spacing) initially within finer columnar grains. The heat from the third layer recrystallizes these finer columnar grains into finer equiaxed grains. This heat can also temper the

Journal of Information Systems Engineering and Management
2025, 10(37s)
e-ISSN: 2468-4376
https://www.jisem-journal.com/

Research Article

pearlite, but because the starting pearlite was finer, the final pearlite in the equiaxed grains will likely be finer than in the lower region. The size of the prior austenite grains plays a crucial role in the final pearlite structure.

Micrography of the P5 sample, depicted in Figure 12, displays similarities with the P4 sample in terms of phase composition and grain morphology. This is in line with what was reported by [7]. However, the lamellar spacing of pearlite colonies in the P5 sample looks like finer than that in the P4. The difference in grain size observed in some layers could be due to factors like cooling rates or specific processing conditions that influence solidification and microstructure development. In general, such observations are important to understand how various processing conditions can affect material properties at microscopic levels. This knowledge is key for optimizing manufacturing techniques to achieve desired mechanical or thermal properties in materials produced through AM methods.

The increased energy input to certain microstructural regions leads to distinct changes in the structure. Even minor variations in energy input can markedly alter the microstructure morphology [14,15]. This sensitivity highlights how critical process parameters are in controlling microstructural evolution during AM.

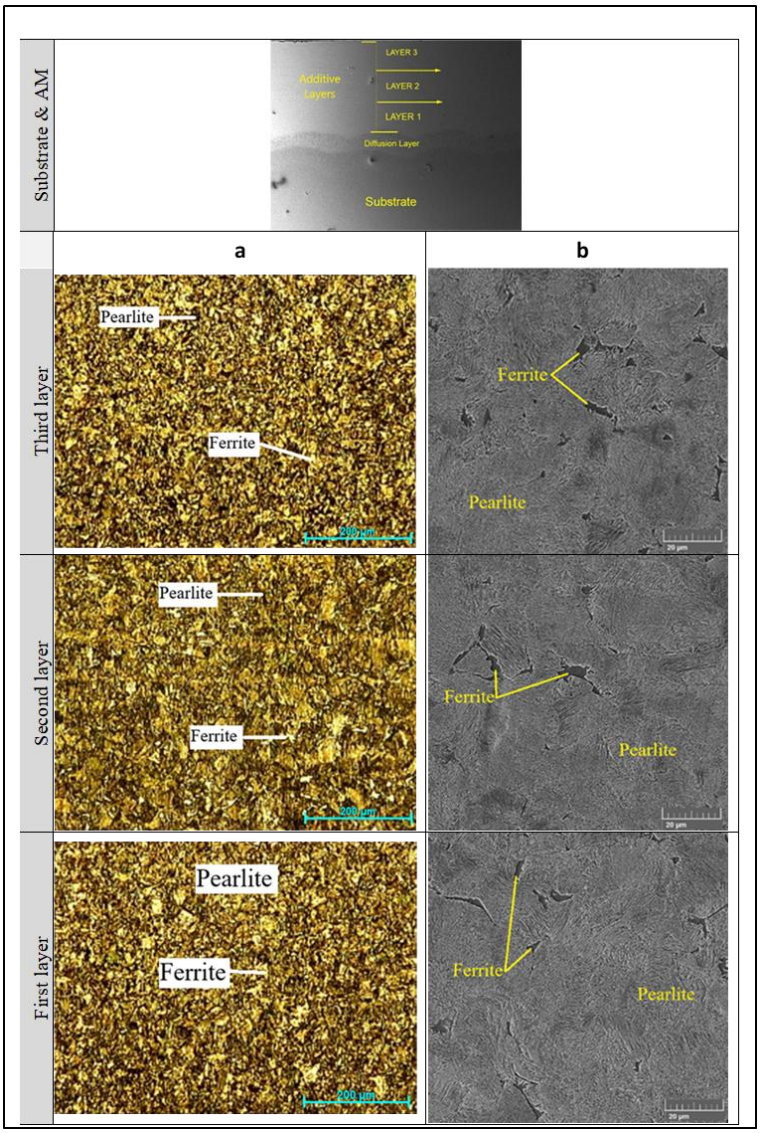

Fig. 12. Micrography for the P5 sample in the different regions along the cross section using (a): OM and (b): SEM.

4.2 Effect of Hot Forging Process on Microstructure

To verify the effect of simultaneous forming and heating, hot forging was applied to the P4 additive. Hot forging of the P4 sample derived from the use of 3HS resulted in a significant reduction in the interlamellar spacing within the

Journal of Information Systems Engineering and Management
2025, 10(37s)
e-ISSN: 2468-4376
https://www.jisem-journal.com/

Research Article

pearlite colonies through the cross-section of the additive material (P436), as illustrated in Figures 13. These figures also depict a reduction in both grain boundary ferrite and ferrite grains, which is attributed to plastic deformation. Additionally, a portion of the microstructure revealed partially spheroidized pearlite. This phenomenon can be explained by the fact that hot forging at 700 °C induces plastic deformation while providing sufficient heat to facilitate the partial transformation of cementite into a semi-spherical shape within the pearlite, which occurs in the intercritical temperature zone.

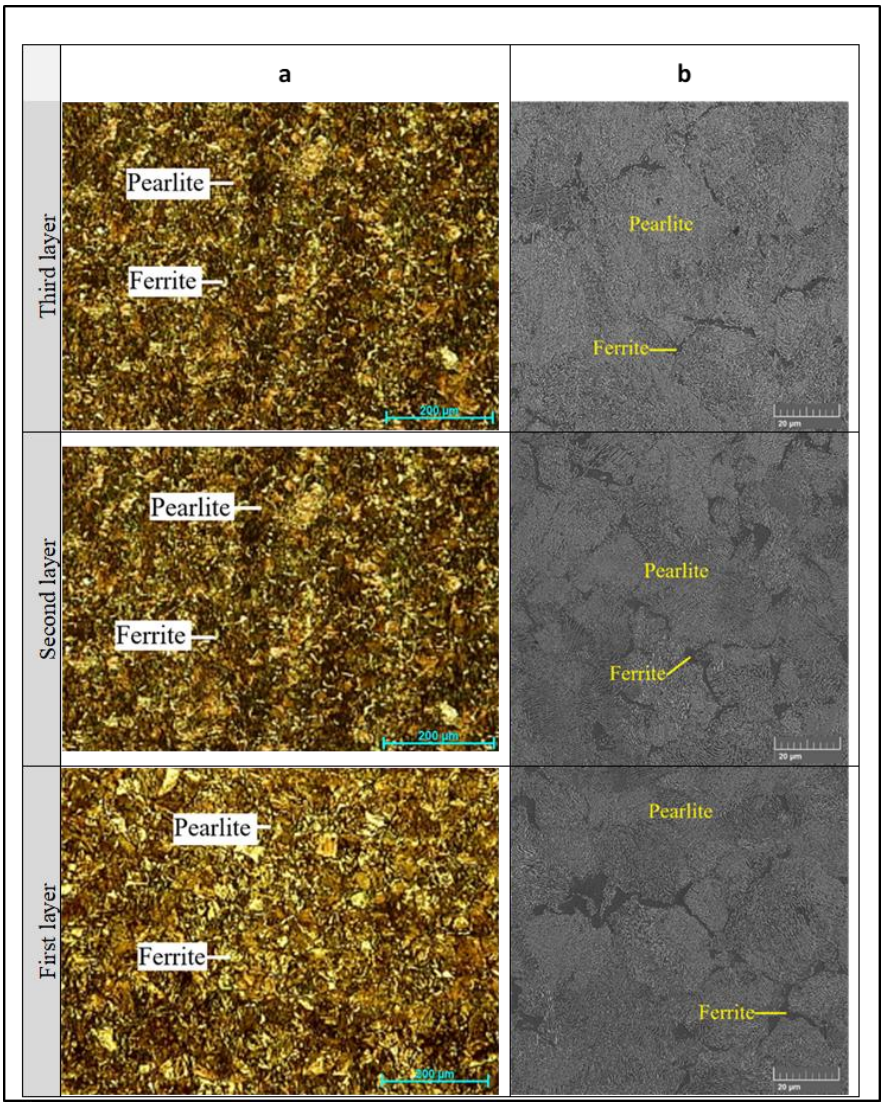

Fig. 13. Micrography for P436 (3HS) sample in the different regions along the cross-section using (a): OM and (b): SEM.

Hot forging causes thermo-mechanical changes that alter the microstructure. According to Micenko et al. (2013) [16], at the intercritical zone (close to A1), the microstructure of pearlitic steel undergoes partial transformation into austenite during heating. As the peak temperature decreases while moving away from A1, spheroidization of cementite within pearlite occurs. The researchers proposed that in this zone, cementite within pearlite colonies undergoes tempering, along with potential spheroidization. Consequently, the microstructure of the additive material contained a notable proportion of spheroidized pearlite. They further hypothesized that the degree of cementite dissolution and spheroidization is influenced by both the peak temperature reached and the duration of exposure to these conditions.

Journal of Information Systems Engineering and Management
2025, 10(37s)
e-ISSN: 2468-4376
https://www.jisem-journal.com/

Research Article

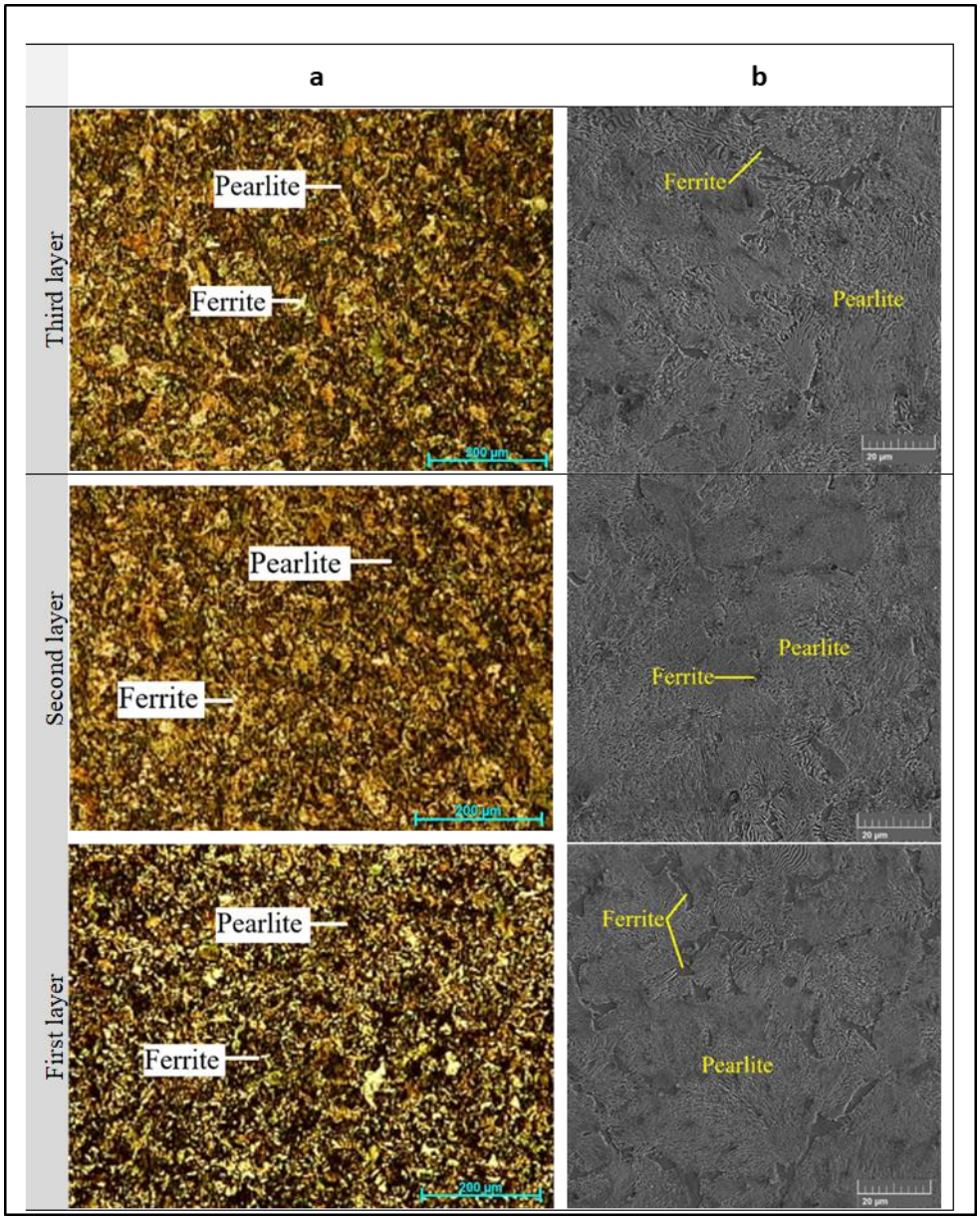

Figure (4.48): Micrography for P456 (5HS) sample in the different regions along the cross-section using (a): OM and (b): SEM.

Increasing the number of hammer strokes to five in P456 resulted in a microstructure similar to that observed in P436, as shown in Figures 14. However, Figures 15 revealed that the content of partially spheroidized pearlite in the microstructure produced with 7HS was noticeably higher. This increase is attributed to the greater number of hammer strokes, which intensified the thermo-mechanical cycle experienced by this sample. Enhanced hammering increases the intensity of the thermo-mechanical cycles, facilitating the transition from lamellar to spherical pearlite structures [17].

Journal of Information Systems Engineering and Management
2025, 10(37s)
e-ISSN: 2468-4376
https://www.jisem-journal.com/

Research Article

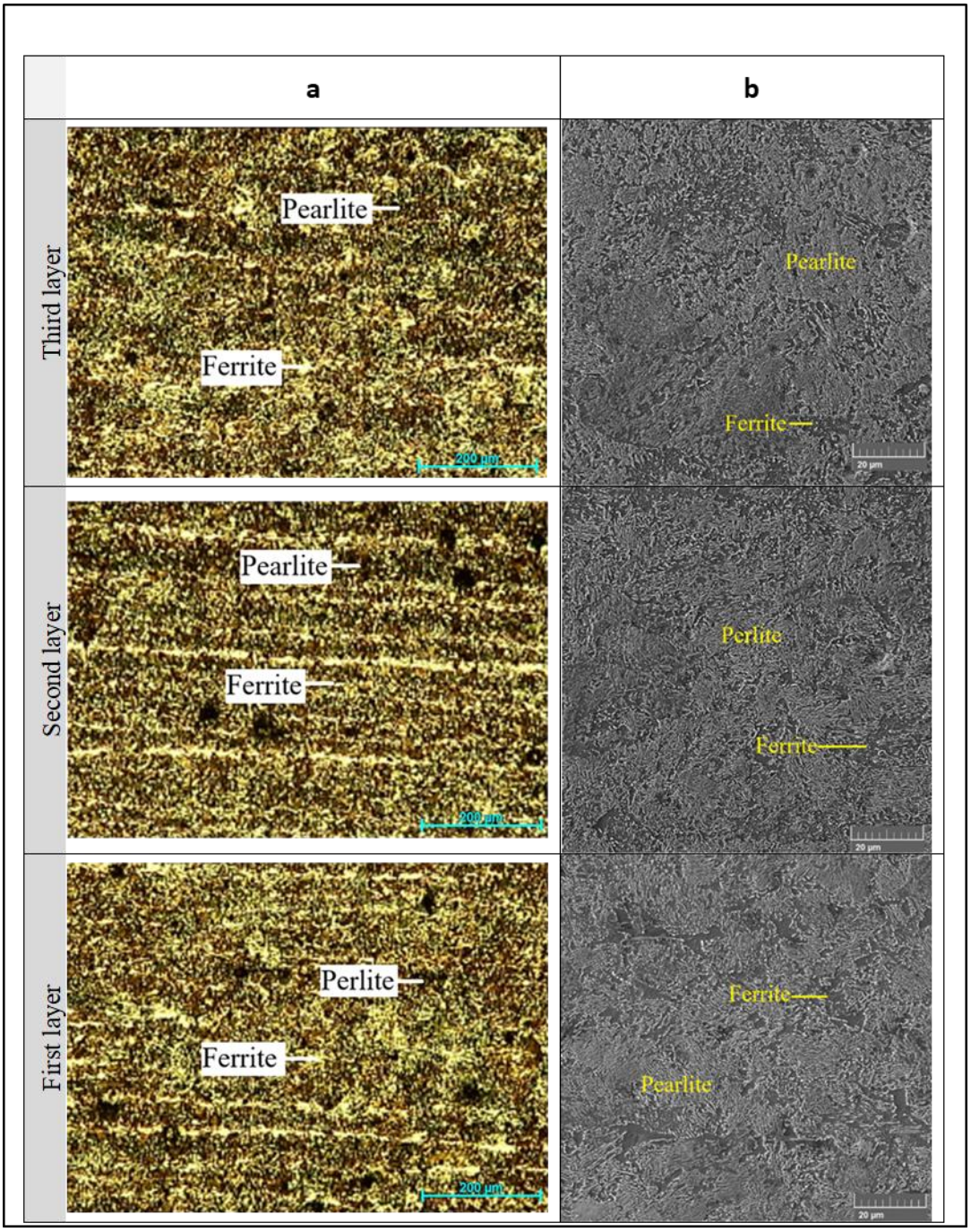

Fig. 15. Micrography for P476 (7HS) sample in the different regions along the cross-section using (a): OM and (b): SEM.

5. CONCLUSIONS

The WAAM samples, built by different deposition patterns, including longitudinal, transverse, right network, oblique and oblique network showed a diversity of microstructure across different regions of the additives in terms of size and morphology. Microscopy generally showed lamellar pearlite as a primary constituent with grain boundary ferrite, accompanied by a smaller fraction of ferrite grains, while some samples showed partially spheroidized pearlite across different regions of the additives. Hot forging introduced a significant reduction in the interlamellar spacing within the pearlite colonies, and in both grain boundary ferrite and ferrite grains, through the cross-section of the additives,

due to plastic deformation. Microscopy has not revealed any defects such as cracks or porosity across any of the additives under study.

REFERENCES

[1] Mohr, S., Khan, O. (2015). "3D Printing and Supply Chains of the Future'. Innovations and Strategies for Logistics and Supply" Chains, pp. 148 – 174.
[2] Sames, W. J., List, F. A., Pannala, S., Dehoff, R. R., &Babu, S. (2016). "The metallurgy and processing science of metal additive manufacturing". International Materials Reviews.
[3] Derekar, K. S. (2018). "A review of wire arc additive manufacturing and advances in wire arc additive manufacturing of aluminium. Materials science and technology" 34(8), 895-916.
[4] Rodrigues, T. A., Duarte, V., Miranda, R. M., Santos, T. G., & Oliveira, J. P. (2019). "Current status and perspectives on wire and arc additive manufacturing (WAAM). Materials" 12(7), 1121. 29.
[5] Ding, D., Pan, Z., Cuiuri, D., & Li, H. (2015). "Wire-feed additive manufacturing of metal components: technologies, developments and future interests". The International Journal of Advanced Manufacturing Technology, 81(1), 465-481.
[6] Wu, B., Pan, Z., Ding, D., Cuiuri, D., Li, H., Xu, J., & Norrish, J. (2018). "A review of the wire arc additive manufacturing of metals: properties, defects and quality improvement". Journal of Manufacturing Processes, 35, 127-139.
[7] Arzaq Al-Roubaiy, Saad Al-Shafaie and Abdul Sameea Jilabi.(2023) "Wire Arc Additive Manufacturing of Steel: Deposition Patterns Effect on Microstructure and Mechanical Properties"., https://doi.org/10.1051/bioconf/20236507010.
[8] A. Yadollahi, N. Shamsaei, S.M. Thompson, D.W. Seely (2015), "Effects of process time interval and heat treatment on the mechanical and microstructural properties of direct laser deposited 316L stainless steel", Mater. Sci. Eng. A 644 171–183, https://doi.org/10.1016/j.msea.2015.07.056.,
[9] Y.M. Wang, T. Voisin, J.T. McKeown, J. Ye, N.P. Calta, Z. Li, Z. Zeng, Y. Zhang, W. Chen, T.T. Roehling, R.T. Ott, M.K. Santala, P.J. Depond, M.J. Matthews, A. V. Hamza, T. Zhu (2018), "additively manufactured hierarchical stainless steels with high strength and ductility", Nat. Mater. 17 63–70.
[10] Van T. L., Henri P. (2020). "On the use of gas-metal-arc-welding additive manufacturing for repurposing low-carbon steel components: microstructures and mechanical properties". Institute of Research and Development, Duy Tan University, Da Nang 550000, Vietnam.
[11] E. Aldalur, F. Veiga, A. Suarez, J. Bilbao, A. Lamikiz. (2020). "High deposition wire arc additive manufacturing mild steel: Strategies and heat input effect on microstructure and mechanical properties". Advanced Manufacturing Department, Paseo Mikeletegi 7, 20009 San Sebasti´an, Spain.
[12] Shukla V, Kumar V, Dixit A. (2023), "Microstructural characteristics and tensile properties of ER70S-6 manufactured by robotic CMT wire-and-arc additive manufacturing". Mater Today: Proc. https:// doi.org/10.1016/j.matpr.02.011
[13] Chunlei Shang, Honghui Wu, Guangfei Pan, Jiaqi Zhu, Shuize Wang, Zhiyuan Liu. (2023), "The Characteristic Microstructures and Properties of Steel-Based Alloy via Additive Manufacturing. Materials" 16 (7), 2696; https://doi.org/10.3390/ma16072696
[14] Ding D, Pan Z, Cuiuri D, Li H, et.al. (2015), "A multi-bead overlapping model for robotic wire and arc additive manufacturing (WAAM)". RoboticsandComputer-IntegratedManufacturing.;31:101 110.
[15] Williams S.W, Martina F, Addison A.C, DingJ, Pardal G, Colegrove P, et.al. (2016), "Wire Arc additive manufacturing. Materials Science Technology".; 32(7):641-647.
[16] Micenko P., Muruganant, Li H. and Xu X. (2013), "Double Dip Hardness Profiles in Rail Weld Heat-affected Zone "- Literature and Research Review Report, CRC for Rail Innovation.
[17] J. Toribio,Francisco-Javier Ayaso,Rocío Rodríguez. (2023), "Pearlite Interlamellar Spacing and Vickers Micro-Hardness in the Necking Region of Cold-Drawn Pearlitic Steel Wires". - Superalloys (Multidisciplinary Digital Publishing Institute) - Vol. 13, Iss: 8 University of Salamanca (USAL), E.P.S., Campus Viriato, Avda. Requejo 33, 49022 Zamora, Spain.